# Programmable Functionalization of Surfactant-Stabilized Microfluidic Droplets via DNA-Tags

Kevin Jahnke,[†,‡] Marian Weiss,[†,‡] Christoph Frey,[†,‡] Silvia Antona,[†,‡] Jan-Willi Janiesch,[†,‡] Ilia Platzman,[†,‡] Kerstin Göpfrich,[*,†,‡] and Joachim P. Spatz[*,†,‡]

†*Max Planck Institute for Medical Research, Department of Cellular Biophysics, Jahnstraße 29, D 69120, Heidelberg, Germany*

‡*Department of Biophysical Chemistry, University of Heidelberg, Im Neuenheimer Feld 253, D 69120 Heidelberg, Germany*

E-mail: kerstin.goepfrich@mpimf-heidelberg.mpg.de; spatz@mr.mpg.de

**Abstract**

Droplet-based microfluidics has emerged as a powerful tool in synthetic biology. For many applications, chemical functionalization of the droplets is a key process. Therefore, we developed a straight-forward and broadly applicable approach to functionalize the inner periphery of microfluidic droplets with diverse reactive groups and components. Instead of covalent modification of the droplet-stabilizing surfactants, our method relies on cholesterol-tagged DNA that self-assembles at the droplet periphery. The cholesterol-tagged DNA serves as an attachment handle for the recruitment of complementary DNA. The complementary DNA can carry diverse functional groups. We exemplify our method by demonstrating the attachment of amine groups, DNA nanostructures, microspheres, a minimal actin cortex and leukemia cells to the droplet periphery. We further show that the DNA-mediated attachment to the droplet periphery is temperature-responsive and reversible. We envision that droplet functionalization via DNA handles will help to tailor droplet interfaces for diverse applications – featuring programmable assembly, unique addressability and stimuli-responsiveness.

## Keywords

Droplet-based microfluidics, DNA nanotechnology, functionalization, cholesterol-tagged DNA, block copolymer surfactant

# Introduction

Physical compartments in the form of emulsion droplets provide an easy to control and self-contained microenvironment. Therefore, droplet-based microfluidics has emerged as a powerful tool to produce such compartments for single cell and deoxyribonucleic acid (DNA) analysis,[1,2] chemical synthesis,[3] drug delivery[4] as well as synthetic cell assembly.[5–7] Many of these applications depend on strategies to functionalize the droplets' inner periphery in order to adjust interactions with the droplet content. This has been achieved by covalent modification of the surfactant molecules themselves, for instance with gold nanoparticles,[8,9] amine groups[10] or carboxyl groups.[11] However, this method is not universally applicable – it depends on the success of the chemical synthesis and can interfere with the stability and the physical properties of the droplets. Moreover, the binding of the functional group to the droplet periphery is irreversible.

DNA nanotechnology,[12] on the other hand can attain the programmable assembly of arbitrary nanoscale architectures like DNA-based lattices,[13] nanopores[14–16] or lid-containing boxes.[17,18] DNA has also been used as a scaffold or linker to assemble secondary components including proteins,[19] gold nanoparticles[20] and liposomes.[21] In addition, networks of emulsion droplets[22,23] or colloid-coated droplets[24] have been created using DNA linkers. Yet in all cases, the linkage was based on biotinylated DNA, which requires additional efforts to graft streptavidin onto the droplet surface. Furthermore, it has never been demonstrated that it is possible to functionalize the interior of block-copolymer surfactant-stabilized droplets with DNA.

Here, we present a broadly applicable method for functionalizing microfluidic droplets utilizing the hydrophobic interaction of cholesterol-tagged DNA with the droplet-stabilizing surfactant. Notably, the interaction of cholesterol with perfluorinated chains has never been described or exploited before. We show that DNA handles can serve as reversible anchoring points for various components including reactive groups, DNA nanostructures, beads, proteins or even cells. The use of off-the-shelf available DNA holds considerable advantages

compared to standard methods for droplet functionalization, including: the broad scope of options for site-directed chemical functionalization, the addressability and programmability due to specific base pairing as well as the reversible stimuli-responsive binding properties of DNA. Therefore, cholesterol-tagged DNA handles bear great potential for various applications in droplet-based microfluidics.

# Results

## Surface-functionalization of surfactant-stabilized droplets with cholesterol-tagged DNA

Droplet-based microfluidics relies on amphiphilic polymer-based agents (surfactants) for the formation of stable water-in-oil or oil-in-water emulsion droplets.[25] Since cholesterol has been used before to tether DNA to lipid membranes,[26] we designed a short 3' cholesterol-tagged DNA oligomer to investigate its self-assembly into the surfactant-layer of microfluidic droplets. The 16 base-long DNA (for DNA sequences see Supporting Information, Table S1) additionally contained a covalently linked fluorophore (Cy3) for visualization purposes. Having tested that the fluorescent dye does not influence the binding properties of the DNA to the droplet periphery (Supporting Information, Figure S5), an Atto488-tagged DNA oligomer without cholesterol served as a control.

Figure 1a shows a sketch of a DNA-containing water-in-oil droplet. The DNA is supplied via the aqueous inlet (2 µM DNA in 10 mM Tris-HCl, 1 mM EDTA, 5 mM $MgCl_2$, pH 8) of a microfluidic droplet-production device (flow focusing PDMS device, see Supporting Information, Figure S2). The confocal image in Figure 1b shows the self-assembled cholesterol-tagged DNA at the water-facing periphery of the surfactant-stabilized in presence of magnesium ions. We find that divalent cations (e.g. 5 mM $MgCl_2$) or increased concentration of monovalent ions (e.g. 100 mM KCl) enhance the efficiency of compartment functionalization, which has previously been observed for the interaction between cholesterol-tagged

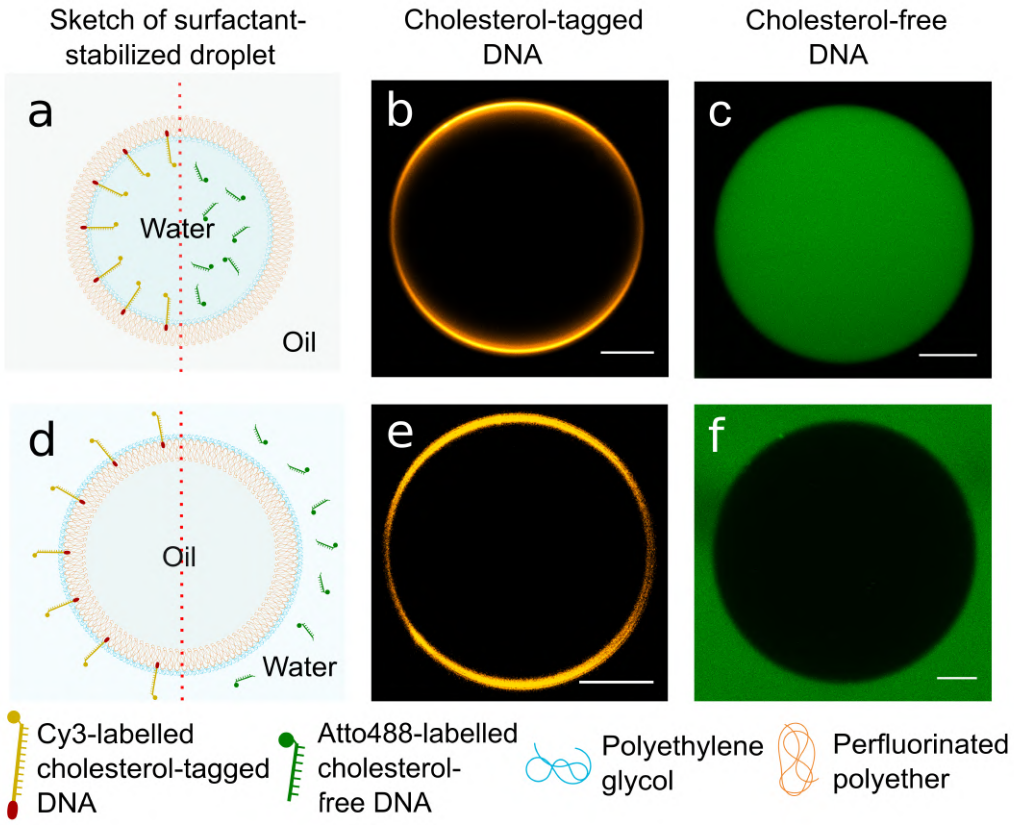


Figure 1: Interaction of cholesterol-tagged and cholesterol-free DNA with surfactant-stabilized droplets. a) Schematic illustration of a water-in-oil droplet (left of red dotted line: with cholesterol-tagged DNA, right side: with cholesterol-free DNA); b,c) Confocal fluorescence images of a water-in-oil droplet with cholesterol-tagged Cy3-labeled DNA ($\lambda_{ex}$ = 561 nm) (b) or with cholesterol-free Atto488-labeled DNA ($\lambda_{ex}$ = 488 nm) added to the internal aqueous phase (c); d) Schematic illustration of an oil-in-water droplet (left side: with cholesterol-tagged DNA, right side: with cholesterol-free DNA); e,f) Confocal fluorescence images of an oil-in-water droplet with cholesterol-tagged Cy3-labeled DNA (e) and cholesterol-free Atto488-labeled DNA (f) added to the external aqueous phase. Whereas cholesterol-tagged DNA self-assembles at the droplet periphery, cholesterol-free DNA remains homogeneously distributed in the aqueous phase (10 mM Tris-HCl, 1 mM EDTA, 5 mM $MgCl_2$, pH 8). Scale bars: 10 µm – independent of the type of fluorophore (see Supporting Information, Figure S5).

DNA and lipid membranes[27] (see Supporting Information, Figure S6). This process happens within milliseconds after droplet formation (see Supporting Information, Text S4 and Video S2). The cholesterol-tagged DNA remains stably attached to the droplet interface for days without affecting droplet stability (Figure S7). This is in accordance with interfacial tension (IFT) measurements, which showed a small but insignificant change of IFT in droplets containing cholesterol-tagged DNA (see Supporting Information, Table S2). In contrast to cholesterol-tagged DNA, cholesterol-free single-stranded DNA is homogeneously distributed in the aqueous phase inside the droplet (Figure 1c, for clarity the aqueous phase was labeled with a fluorescent dye in Figure S3). This proves that the self-assembly of the DNA at the droplet periphery is due to hydrophobic interactions between the DNA-linked cholesterol moiety and the surfactant molecules – rather than electrostatic interactions between DNA and surfactants. To broaden the range of possible applications of DNA-functionalized droplets, we demonstrate that our system also works for oil-in-water droplets (see Materials and Methods). Figure 1e shows cholesterol-tagged DNA attached to the aqueous exterior of the droplet, while the cholesterol-free DNA remains homogeneously distributed in the aqueous phase surrounding it (Figure 1f).

To gain more insights into the interaction of the cholesterol-tagged DNA and the droplet periphery, we set out to probe the mobility of the DNA in the surfactant layer. To this end, we performed fluorescence recovery after photobleaching (FRAP) measurements with the water-in-oil droplets containing cholesterol-tagged DNA. A confocal plane at the bottom of the droplet was selected and a circular bleaching area (5 µm diameter) was defined. The measurement procedure is illustrated in Figure 2a. It consists of a pre-bleaching time span (i), followed by bleaching of the circular area (ii), and a recovery period (iii). The mean intensities acquired from the images before bleaching were used to calculate normalized intensity values. From an exponential fit of the normalized recovery intensities, the diffusion coefficient was calculated (Supporting Information, Text S2).

A representative FRAP intensity curve as a function of time is shown in Figure 2b. First,

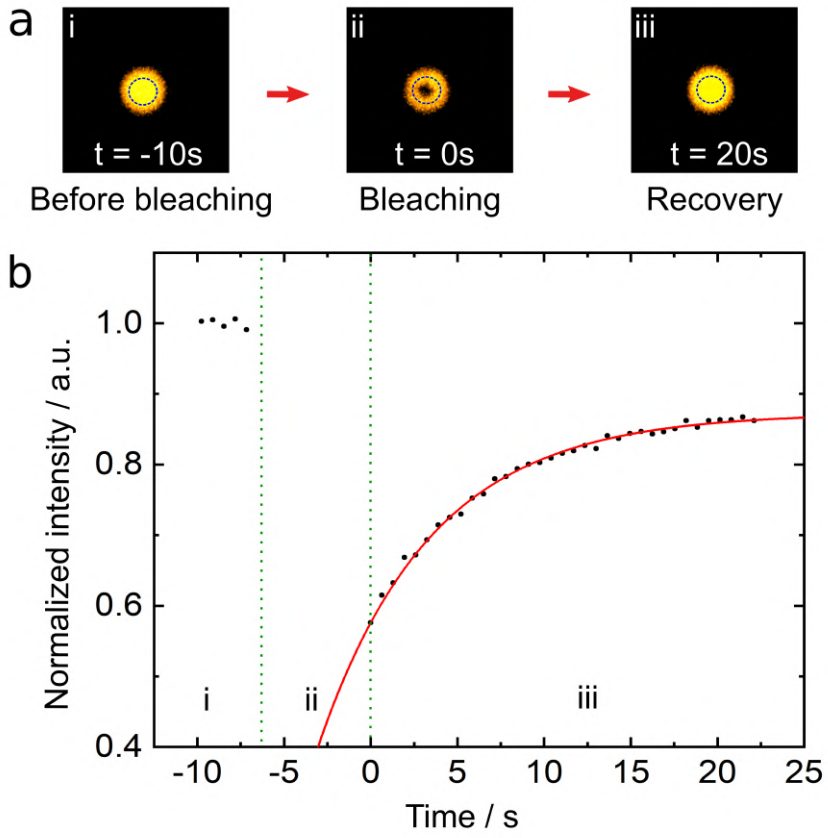


Figure 2: FRAP measurements of microfluidic water-in-oil droplets functionalized with cholesterol-tagged Atto488-labeled single-stranded DNA. a) Confocal fluorescence images of a droplet (bottom plane) i: before bleaching, ii: directly after bleaching (circular bleaching area clearly visible, $\lambda_{ex} = 488$ nm), and iii: after recovery. The bleached area is highlighted with a blue dashed circle. b) Representative recovery curve. Mean normalized intensity values within the bleaching area are plotted as a function of time. The red line represents an exponential fit, which was used to determine the diffusion coefficient, here: $D$ =0.412 µm$^2$ s$^{-1}$. The three phases of the experiment (i-iii) are indicated.

it should be noted that the cholesterol-tagged DNA is indeed diffusive when incorporated into the droplet periphery (Figure 2a). We obtained a diffusion coefficient of $D = (0.41 \pm 0.01)$ µm$^2$ s$^{-1}$ based on FRAP measurements performed on 17 independent droplets. This value is comparable to the diffusion coefficient of block copolymer surfactants,[6] but two orders of magnitude smaller than typical diffusion coefficients of high-cholesterol content lipid membranes.[28] We further demonstrated that the diffusion coefficient increases with decreasing surfactant concentrations (Supporting Information, Text S3 and Figure S8). This is to be expected since a denser surfactant layer will confine the mobility of the cholesterol-tagged DNA.

## Droplet functionalization via DNA handles

In order to verify that the single-stranded DNA handles at the droplet periphery are accessible for duplex formation, a complementary Cy5-labeled DNA sequence (without cholesterol-tag) was supplied via the aqueous phase during droplet production. In the presence of the Cy3-labeled cholesterol-tagged DNA handles the cholesterol-free DNA strand was found at the droplet periphery, indicating successful duplex formation (Supporting Information, Figure S9). Without the DNA handles, the cholesterol-free DNA was homogeneously distributed within the droplet as shown in Figure 1c. This observation is independent of the type of fluorophore label (Supporting Information, Figure S5).

With this system in place, we made use of the large toolbox of chemical modifications available for DNA and functionalized the droplet periphery with a variety of components. The easiest and at the same time broadly applicable modification is the attachment of commonly used functional groups. One example is a commercially available amine-terminated DNA oligo (see Materials and Methods). We used confocal fluorescence imaging to confirm the successful attachment of the amine-modified DNA (labeled with Atto488) to the unlabeled DNA handles at the droplet periphery (see Figure 3a). As a next step, we demonstrated that the DNA handles can also serve as anchoring points for DNA nanostructures.

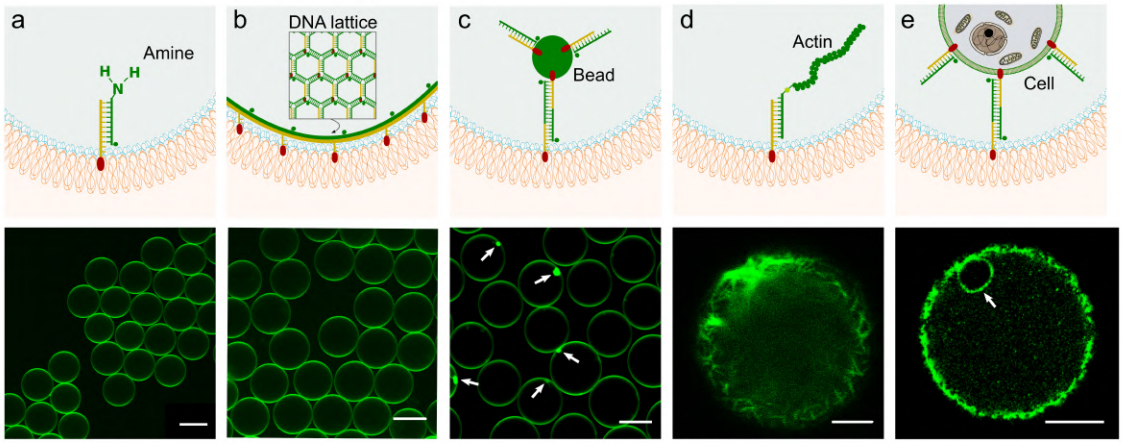


Figure 3: Microfluidic water-in-oil droplets can be functionalized with various components via complementary DNA-tags. Schematic illustrations in the top row show a close-up of a single cholesterol-tagged DNA handle attached to the droplet periphery interacting with the added component. The bottom row shows confocal fluorescence images of entire water-in-oil droplets, in groups or as a close up of a single droplet. Added components were as follows. a) complementary amine-tagged DNA (Atto488-labeled); b) an Atto488-labeled hexagonal DNA-lattice; c) plain multifluorescent polystyrene microspheres grafted with complementary FITC-labeled DNA ($\lambda_{ex}$ = 488 nm) via hydrophobic interactions. The white arrows indicate the position of polystyrene microspheres. d) filamentous actin (containing 10 mol% biotinylated actin and 1 mol% Atto488-labeled actin). The actin filaments were functionalized with complementary biotinylated DNA via biotin-streptavidin linkage; e) Leukemia cell (K562) incubated with complementary cholesterol-tagged DNA. The white arrow indicates the position of the cell. The cholesterol-tagged DNA is localized at the lipid membrane of the cells and through two complementary DNA strands binds the cholesterol-tagged DNA on the periphery of the droplets (see Figure S17). Scale bars in the lower row of images are: 30 µm in a and b, 20 µm in c and e, 5 µm in d. For DNA sequences see Supporting Information, Table S1.

For this purpose, we assembled a hexagonal Atto488-labeled DNA lattice[29] (see Supporting Information, Figure S1 and Table S1). Its adhesion to the compartment periphery is visible in the confocal image in Figure 3b. To probe the formation of an interconnected lattice structure, we performed FRAP measurements on droplets containing a fluorophore-labeled DNA lattice. We observe a significantly slower recovery of the fluorescence than for the single stranded DNA ($D = 0.33 \pm 0.03\,\mu m^2\,s^{-1}$ vs. $D = 0.41 \pm 0.01\,\mu m^2\,s^{-1}$), which is consistent with the formation of a large assembly at the droplet periphery.

Beyond functional groups and DNA nanostructures, we employed the cholesterol-tagged DNA handles as attachment points for polystyrene microspheres with a diameter of 2 µm (see Materials and Methods). For this purpose, we designed a longer DNA-based linker, which provides more space between the microspheres and the droplet periphery. The linker is made up of two cholesterol-tagged DNA duplexes that each have a single-stranded DNA overhang. These overhangs can interconnect, creating a strong linker, as shown in the illustration in Figure 3c (for sequences see Supporting Information, Table S1). This linking method requires just one rather than two different cholesterol-tagged DNA sequences, making it more cost-effective than the direct link. The microspheres were first incubated with one of the cholesterol-tagged duplexes. As shown in Figure S11 (Supporting Information), the DNA adheres to the surface of the microsphere. The second cholesterol-tagged DNA duplex served as an attachment point at the droplet periphery, binding DNA-coated microspheres via the single-stranded DNA overhang. As visible in the confocal image in Figure 3c, the microspheres attached to the droplet periphery, whereas when DNA was missing, they were distributed randomly (see Supporting Information, Figure S12). Note that it is also possible to use modified microspheres of different sizes carrying functional groups (see Supporting Information, Figure S13). Next, we went one step further by attempting to assemble a minimal actin cortex inside the microfluidic droplet.[30–32] Again, our approach relied on the DNA-handle-system, which we modified to link actin filaments to the droplet periphery. We first polymerized a mixture of G-actin monomers that were modified with

either Alexa488 or biotinylation or that were left unmodified into up to 5 µm long filaments. This mixture was then added to a solution containing biotinylated DNA and streptavidin and encapsulated into the droplets. The confocal image in Figure 3d shows that we were successful in binding actin filaments to the droplet periphery, building up a well-defined minimal actin cortex. The filaments are arranged in a spherical manner at the droplet periphery, whereas excess labeled monomers can be found in the droplet lumen. In a control without the DNA handles, the actin filamets remained homogeneously distributed within the droplet (Supporting Information, Figure S14). In living cells, the binding of actin to the periphery involves a multitude of proteins.[33] We have achieved an artificial imitation using much fewer components – demonstrating the potential of DNA-based linkers in bottom-up synthetic biology.[34]

Increasing the level of complexity one step further, we went from the attachment of purified proteins to living cells. Droplets have previously been used as microreactors for cells to perform high-throughput single cell analysis.[35–39] Nonetheless such applications often require controlled interactions between encapsulated cells and the droplet periphery.[9,40] We therefore set out to test if our DNA-handle-system is capable of anchoring living cells at the droplet periphery. We first incubated myelogenous leukemia cells (K562) with a cholesterol-tagged DNA duplex as used previously for the microspheres. The linkage via four rather than two DNA strands ensures a larger distance between the cell and the droplet periphery, leaving the cells in their native environment and avoiding unwanted interactions with the surfactant molecules. The confocal images in Figure S17 (Supporting Information) show the DNA localized at the lipid bilayer membrane of the cells. As with the microspheres, we could bind the cells to the DNA-functionalized droplets periphery via the single-stranded overhang on the DNA duplex. Figure 3e shows an encapsulated K562 cell, which was attached to the droplet periphery via the described DNA linkers. Cell viability within the droplets was assessed for 100 min upon encapsulation (see Supporting Information, Figure S16). 95 % of cells were still viable after the observation period in the presence as well as in the absence

of the DNA handles, indicating that the cholesterol-tagged DNA showed no cytotoxic effect. Increasing the concentration of cells, we also observed DNA-mediated cell-cell interactions, building up droplet-spanning multicellular clusters (see Supporting Information, Figure S19). The fluorescent DNA clusters in the droplet lumen, visible in Figure 3e, likely result from the use of cell culture medium containing proteins and hydrophobic molecules with which the cholesterol can interact. Furthermore we showed that our DNA anchoring method is also applicable for different cell lines (see Supporting Information, Figure S15-19). All these experiments exemplify the ability of DNA to act as a linker between the droplet periphery and various components making it a universally applicable tool for the functionalization of surfactant-stabilized droplets.

## Temperature-responsive reversibility

For many applications, stimuli-responsive droplet functionalization is highly desirable as it offers a route to detect and sort the content of microfluidic droplets. This especially concerns applications such as droplet-based cell sorting,[41] drug delivery,[42] DNA sequencing[43] or material synthesis.[44] In particular, the field of bottom-up synthetic biology will benefit from the dynamic control over the organization of intracellular components.[34,45] These applications require mechanisms to turn interactions with the droplet periphery on and off upon demand. With the DNA-handle-system, we can make use of the temperature-dependency of Watson-Crick base pairing between strands of DNA to achieve stimuli-responsive reversibility of the binding.

We carried out temperature cycling experiments during which the DNA-containing droplets were placed on a temperature-controlled stage during confocal imaging. These experiments can reveal whether a) the cholesterol-tagged DNA is stable at the periphery even at elevated temperatures and b) the complementary DNA (which can carry diverse functional groups, as shown in Figure 3) can be reversibly detached from the periphery. Figure 4a shows confocal fluorescence images of the cholesterol-tagged DNA (top row, Atto488-labeled) and the

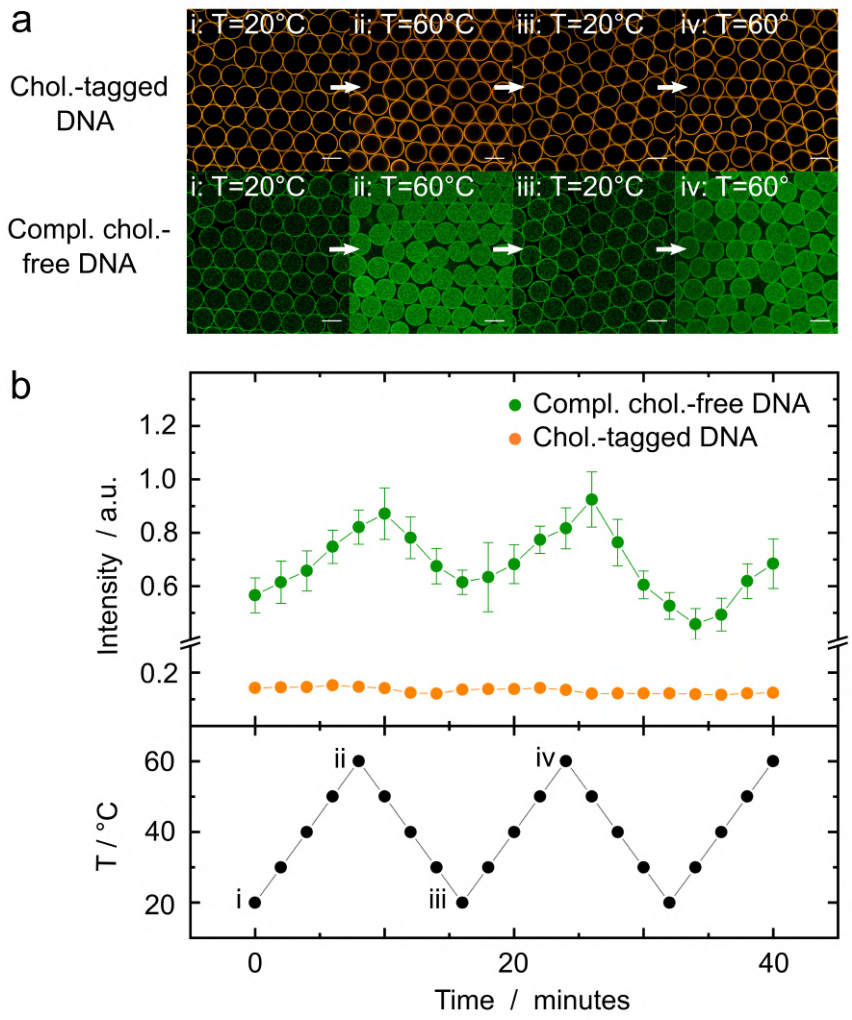


Figure 4: Temperature-responsive reversibility of droplet functionalization. a) Confocal fluorescence images of cholesterol-tagged DNA (top row, labeled with Atto488, $\lambda_{ex}$ =488 nm) and complementary DNA (bottom row, labeled with ROX, $\lambda_{ex}$ =580 nm) in the same surfactant-stabilized droplets for two consecutive temperature cycles (heating from 20 °C to 60 °C, cooling to 20 °C, then heating to 60 °C). Scale bars: 30 µm. b) Average fluorescence intensity within the droplets (periphery excluded) during the temperature cycles for the cholesterol-tagged DNA (orange) and its complementary strand (green) as a function of time. The temperature is plotted below. Error bars for the complementary strand correspond to the standard deviation of the analysis of 20 droplets (error bars for the cholesterol-tagged strand are too small to be visible). The time points when the four images shown in a) were taken are indicated. The complementary strand binds to the cholesterol-tagged DNA handle at the periphery at lower temperatures. Above the melting temperature of the duplex, the complementary cholesterol-free DNA was homogeneously distributed within the aqueous phase of the same droplet (10 mM Tris-HCl, 1 mM EDTA, 5 mM $MgCl_2$, pH 8). Furthermore, the cholesterol-tagged DNA anchor remained at the droplet periphery, showing the high entropical benefit of cholesterol-insertion into the surfactant layer. For DNA sequences, see Supporting Information, Table S1.

complementary DNA (bottom row, ROX-labeled) encapsulated together in a droplet, during temperature cycling experiments. While the cholesterol-tagged DNA remains bound to the periphery at temperature between 20 °C and 60 °C, the complementary DNA detaches at elevated temperatures. The melting temperature of the DNA duplex (i.e., the temperature when half of the complementary DNA should be unbound) was calculated to be approximately 28.3 °C.[46] In Figure 4b, we plotted the average fluorescence intensity within droplets (periphery excluded) and the applied temperature as a function of time. When the fluorophore-tagged DNA was bound to the periphery this value was low but it increased as more DNA detached. The intensity was measured for cholesterol-tagged Atto488-labeled DNA (orange) as well as for the complementary ROX-labeled DNA (green). The cholesterol-tagged DNA is found at the periphery at all times and temperatures – hence the fluorescence intensity in the droplet lumen remains low. This shows that the hydrophobic interaction between surfactant and cholesterol is stronger than the sum of the hydrogen bonds between all DNA bases. The insertion of the cholesterol-tagged DNA is entropically beneficial and stable. In contrast, the plot clearly shows the periodic oscillations of the complementary DNA with each temperature cycle. This means that the complementary DNA is located mainly at the periphery at 20 °C and found within the droplet lumen at higher temperatures. This is in agreement with the calculated melting temperature of the employed DNA of 28.3 °C.[46] Because of the low melting temperature, even at 20 °C, not all of the complementary DNA may be bound. The binding can be enhanced by using longer DNA sequences with higher melting temperatures as we did in Figure 3. In addition, hysteresis effects can be observed by comparing the intensity maxima with the temperature, according to which the maximum is reached when the temperature drops back to 50 °C. This is conclusive considering that the system needs some time to equilibrate, which becomes more clear, when looking at the temperature of the heating plate as depicted in Figure 4. From these experiments, we can conclude that the functionalization of the droplet periphery is reversible.

# Conclusion

In the present study we demonstrated a versatile method for the functionalization of microfluidic droplets using DNA-tags. We showed that cholesterol-tagged DNA self-assembles into the periphery of surfactant-stabilized water-in-oil and oil-in-water droplets due to the hydrophobic interactions between the surfactant molecules and the cholesterol-tag at the interface between oil and water. Furthermore, by means of FRAP measurements we found that the DNA anchored in the surfactant layer is diffusive with $D = (0.41 \pm 0.01)\mu m^2\,s^{-1}$ and that the diffusivity depends on the surfactant concentration. Importantly, we proved that the DNA strand attached to the periphery remains fully addressable. It can act as a sequence-specific and programmable anchor for a variety of components attached to a complementary DNA strand. By creating a link between the droplet periphery and one of either amine-groups, a DNA lattice, plain microspheres, actin filaments or living cells, we showcased the versatility of our DNA handles. In principle, the system can be extended to any other functional group and component that can be linked to DNA, e.g. thiol-groups, adenylation, phosphorylation, various DNA nanostructures, gold nanoparticles, lipid vesicles or other types of proteins and cells. Conveniently, various functional groups covalently linked to DNA are commercially available. Lastly, we showed that droplet functionalization as a result of DNA duplex formation, is temperature dependent and fully reversible. The temperature at which unbinding happens is fully controllable by choosing a DNA sequence with the desirable melting point. In addition, other stimuli-responsive DNA motifs, like pH-[47–49] and light-responsive[50] elements, could be incorporated to achieve reversibility of droplet-functionalization. All in all, this study shows the potential of DNA handles to specifically and reversibly functionalize surfactant-stabilized droplets for diverse applications in droplet-based microfluidics.

# Experimental Section

## Design and assembly of DNA-tags

A set of random fixed-length DNA sequences was generated in MATLAB (MathWorks, Inc.) using the *randseq* command. The sequences were analyzed in NUPACK[51] and chosen such as to provide stable base-pairing with complementary sequences at room temperature and an overall low tendency to form secondary structures amd self-dimers. The selected DNA oligos, listed in Table S1, were purchased from Integrated DNA Technologies, Inc. or biomers.net GmbH. HPLC purification was performed for DNA oligos carrying modifications (Cy3, Cy5, FITC, ROX, Atto488, cholesterol-TEG, biotin or amine). The DNA oligos were diluted in Milli-Q water at a stock concentration of 100 µM, aliquoted and stored at −20 °C until use. Before the experiment, cholesterol-tagged DNA oligos were heated to 60 °C for 5 minutes to reduce aggregation. A concentration of 2 µM of each oligonucleotide was used in the aqueous solution, if not stated otherwise.

## Microfluidic formation of DNA-functionalized surfactant-stabilized water-in-oil droplets

Microfluidic PDMS-based (Sylgard 184, Dow Corning, USA) devices for the formation of water-in-oil droplets were produced and assembled as described previously.[6] Figure S2 shows the layout of the devices used here, which feature a water and an oil channel that meet at a flow-focusing T-junction for droplet formation. The aqueous phase is made up of Milli-Q water containing 5 mM $MgCl_2$, 1x Tris-EDTA buffer, pH 8 (Buffer 1) and 2-4 µM DNA unless otherwise specified. The oil-phase contains either 2 wt% of Perflouro-polyether-polyethylene glycol (PFPE-PEG) block-copolymer fluorosurfactants (PEG-based fluorosurfactants from Ran Biotechnologies, Inc.) or 2.5 mM of a custom synthesized triblock-copolymer PFPE-PEG-PFPE triblock-copolymer surfactant[9,52] dissolved in HFE-7500 oil (from DuPont). The flow rates were generally set to 900 µl $h^{-1}$ for the oil phase and 300 µl $h^{-1}$ for the

water phase using syringe pumps PUMP 11 ELITE (Harvard apparatus, USA). The fluids were injected with 1 ml syringes (Omnifix, B.Braun, Germany) connected by a cannula (Sterican®0.4 x 20 mm, BL/LB, B.Braun, Germany) and PTFE-tubing (0.4 x 0.9 mm, Bola, Germany). To observe the production process, an Axio Vert.A1 (Carl Zeiss AG, Germany) inverse microscope was used. With these settings, homogeneous droplets with a diameter of approximately 30 µm were produced at a rate of 1 kHz.

## Formation of surfactant-stabilized oil-in-water droplets

Oil-droplets with a surrounding aqueous phase were produced manually by shaking. For this purpose, 10 µl of the surfactant-containing oil phase were added to 700 µl of the DNA-containing aqueous solution. The composition of the oil and the water phase were chosen as before. The probe was manually shaken until oil-in-water droplets formed (visible as a milky emulsion layer).

## High-speed fluorescence imaging

For imaging the production of water-in-oil droplets containing Cy3-labeled cholesterol-tagged or cholesterol-free DNA (10 µM), a fluorescence illuminator (HBO 100, Carl Zeiss AG, Germany), FS43HE Filter (Carl Zeiss AG, Germany) and a 40x objective (LD Plan-Neofluar 40x/0.6 Korr, Carl Zeiss AG, Germany) were used. For imaging purposes, lower flow rates (30 µl $h^{-1}$ for aqueous phase and 120 µl $h^{-1}$ for oil phase) were chosen. The Videos S1-S3 were recorded with a fluorescence sensitive high-speed camera (HiCam Fluo, Lambert Instruments, Netherlands), at a resolution of 640x480 pixels and a framerate of 4087 fps for the Video S1 and 1000 fps for video S2 and S3. The integrated intensifier module of the camera was used with an MCP gain of 1.11 V and a gate width of 4 ms. The recorded videos were modified with ImageJ (NIH, brightness and contrast adjusted for all videos with the same parameters).

## Confocal fluorescence microscopy

A confocal laser scanning microscope LSM 800 (Carl Zeiss AG) was used for confocal imaging. The pinhole aperture was set to one Airy Unit and experiments were performed at room temperature. The images were acquired using a 20x (Objective Plan-Apochromat 20x/0.8 M27, Carl Zeiss AG) and a 63x immersion oil objective (Plan-Apochromat 63x/1.40 Oil DIC, Carl Zeiss AG). Images were analyzed with ImageJ (NIH, brightness and contrast adjusted).

## FRAP measurements

FRAP measurements were performed using a Leica SP5 confocal microscope (Leica Microsystems, Germany), equipped with an argon laser and a 63x oil-immersion objective (HCX PL APO 63x/1.40-0.60; Leica Microsystems GmbH). Surfactant-stabilized water-in-oil droplets functionalized with single-stranded DNA (DNA #1 in Table S1, with an Atto488-tag on the 5' end and a cholesterol-tag on the 3' end) were sealed in an observation chamber. Subsequently, a bleaching spot with a radius of 2.5 µm was defined at the confocal plane at the bottom of the droplet. Using the FRAP-WIZZARD, five images were recorded before bleaching, followed by 6.5 s bleaching and the acquisition of 35 images after bleaching. Representative images are shown in Figure 2. The frame rate was set to 0.65 s. The diffusion coefficient, which was averaged from 17 independent measurements, was derived from the recorded images using a custom-written MATLAB (MathWorks, Inc.) code as detailed in the Supporting Information.

## Attachment of amine groups, DNA nanostructures, beads, actin and cells to the DNA handles

For all attachment experiments, confocal imaging was carried out as described before.

*Amine groups:* A DNA oligo with an amine-group at the 3' end and an Atto488-label at the 5' end (DNA #3, Table S1) was purchased from Biomers. It was mixed with complementary

cholesterol-tagged DNA (DNA #1) at an equimolar concentration of 2 µM in the standard buffer (Buffer 1) and encapsulated in microfluidic droplets as described.

*DNA nanostructures:* To demonstrate the attachment of DNA nanostructures to the droplet periphery, we chose a hexagonal DNA lattice composed of 3 unique DNA sequences.[29] We modified one with a 3' cholesterol-tag (DNA #4ii, Table S1), a second one with a 5' Atto488-tag (DNA #4i) and left a third one without modification (DNA #4iii, all from Biomers) (see Figure S1). The three strands were mixed in Buffer 1 at a concentration of 2 µM and heated to 60 °C for 10 minutes using a thermocycler (BioRad) before microfluidic encapsulation.

*Polystyrene beads:* Plain polychromatic polystyrene microspheres with a diameter of 2 µm were purchased from Fluoresbrite$^{TM}$, Polysciences, Inc. The beads were mixed with 4 µM DNA #7 and 2 µM DNA #8 and #9 (Table S1) at a concentration of approximately $10^6$ µl$^{-1}$ in Buffer 1 before droplet production. Filter-free devices were used to prevent the beads from blocking the channel.

*Actin:* Actin (Cytoskeleton, Inc.) was stored in a buffer containing 2 mM TRIS/HCl, pH 8, 0.2 mM $CaCl_2$, 0.2 mM ATP, 0.005 % $NaN_3$ and 0.2 mM DTT, at -80 °C. The actin monomers were mixed with 10 mol% biotinylated-actin (cytoskeleton) and 1 mol% of Alexa488-labeled actin (LifeTechnologies). Before encapsulation, the monomers were polymerized into 5-10 µm sized filaments using an actin polymerization buffer (2.0 mM TRIS/HCl pH 8, 20 mM $MgCl_2$, 0.2 mM $CaCl_2$, 0.5 mM ATP, 0.005 % $NaN_3$ and 0.2 mM DTT). After one hour of incubation (at room temperature), streptavidin (for biotin-binding) was added in 5-fold excess (10 µM) to the F-actin to enable the binding of biotinylated DNA (DNA #6, Table S1). After incubation, the solution was centrifuged at $10^6$ g (Beckman Coulter Optima$^{TM}$MAX-XP Ultracentrifuge) for 1h and the F-actin pellet was afterwards resuspended in HEPES pH 8.2 buffer to a final actin concentration of 80 µM. The complementary biotinylated and the cholesterol-tagged DNA were supplied via a second aqueous inlet in the microfluidic device at a concentration of 8 µM, yielding a one-to-one ratio of biotinylated F-actin and DNA strands. To prevent blocking, encapsulation experiments were performed using filter-free

microfluidic devices.

*Leukemia and Jurkat cells:* Myelogenous leukemia K562 cells (ATCC®CCL-243™) were cultured in Iscove's Modified Dulbecco's Medium (IMDM) (ATCC®30-2005™) containing 10 % fetal bovine serum in a humidified incubator at 37 °C and 5 % $CO_2$. Jurkat, Clone E6-1(ATCC®TIB-152™) were cultured in RPMI-1640 (Thermo Fisher Scientific) containing 10 % fetal bovine serum and 1 % penicillin-streptomycin in a humidified incubator at 37 °C and 5 % $CO_2$. For both cell lines the medium was changed every two days and cells were maintained at a cell density of 2x$10^5$ cells/ml. Prior to the experiment, cells were harvested, centrifuged and re-suspended in culture media at a final concentration of $10^6$ cells/ml. 4 µM cholesterol-tagged DNA was added to the cell suspension before encapsulation. Because of typical cell sizes of 10-15 µm a filter-free device with 80 µm wide (instead of 30 µm) channels was used, resulting in droplets with a diameter of 80 µm. For cell viability experiments propidium iodide (PI, Thermo Fisher Scientific) was added in a concentration of 1 µg µ$L^{-1}$ to the culture media of the cell suspension.

## Thermal cycling experiments

DNA strands #10 and #11 were encapsulated in microfluidic droplets containing with Buffer 1. ROX was chosen as a fluorophore due to its known temperature stability.[53] Droplets were sealed in an observation chamber and imaged using a Leica SP5 microscope with a 60x oil immersion objective. The temperature was increased with a temperature-controlled microscope stage (Tokai Hit ThermoPlate TP-110) from 20 °C to 60 °C and subsequently decreased in steps of 10 °C, each lasting 3 minutes. This cycle was then repeated 2.5 times. The region of interest (ROI) was changed for every temperature step to avoid bleaching. Fluorescence intensities within 20 droplets were analyzed using ImageJ.

## Supporting Information Available

## Acknowledgements

The authors thank Cornelia Weber for useful discussions and for providing actin filaments. The authors acknowledge funding from the European Research Council, Grant Agreement no. 294852, SynAd and the MaxSynBio Consortium, which is jointly funded by the Federal Ministry of Education and Research of Germany and the Max Planck Society. They also acknowledge the support from the SFB 1129 of the German Science Foundation and the Volkswagen Stiftung (priority call 'Life?'). J.P.S. is the Weston Visiting Professor at the Weizmann Institute of Science and part of the excellence cluster CellNetworks at the University of Heidelberg. K.G. received funding from the European Unions Horizon 2020 research and innovation program under the Marie Skłodowska-Curie grant agreement No 792270. The Max Planck Society is appreciated for its general support.

# References


[1] H. N. Joensson, H. Andersson Svahn, *Angew. Chem., Int. Ed.* **2012**, *51*, 12176–12192.

[2] A. R. Abate, T. Hung, R. A. Sperling, P. Mary, A. Rotem, J. J. Agresti, M. A. Weiner, D. A. Weitz, *Lab Chip* **2013**, *13*, 4864.

[3] K. S. Elvira, X. C. i Solvas, R. C. R. Wootton, A. J. deMello, *Nat. Chem.* **2013**, *5*, 905–915.

[4] G. T. Vladisavljevic, N. Khalid, M. A. Neves, T. Kuroiwa, M. Nakajima, K. Uemura, S. Ichikawa, I. Kobayashi, *Adv. Drug Delivery Rev.* **2013**, *65*, 1626–1663.

[5] Y.-C. Tan, K. Hettiarachchi, M. Siu, Y.-R. Pan, A. P. Lee, *J. Am. Chem. Soc.* **2006**, *128*, 5656–5658.

[6] M. Weiss, J. P. Frohnmayer, L.T. Benk, B. Haller, J.-W. Janiesch, T. Heitkamp, M. Börsch, R. B. Lira, R. Dimova, R. Lipowsky, E. Bodenschatz, J.-C. Baret, T. Vidakovic-Koch, K. Sundmacher, I. Platzman, J. P. Spatz, *Nat. Mater.* ***2017***, *17*, 89–96.

[7] B. Haller, K. Göpfrich, M. Schröter, J.-W. Janiesch, I. Platzman, J. P. Spatz, *Lab Chip* **2018**, *18*, 2665–2674.

[8] H. Heinz, C. Pramanik, O. Heinz, Y. Ding, R. K. Mishra, D. Marchon, R. J. Flatt, I. Estrela-Lopis, J. Llop, S. Moya, R. F. Ziolo, *Surf. Sci. Rep.* **2017**, *72*, 1–58.

[9] I. Platzman, J.-W. Janiesch, J. P. Spatz, *J. Am. Chem. Soc.* **2013**, *135*, 3339–3342.

[10] M. Li, W. Jiang, Z. Chen, S. Suryaprakash, S. Lv, Z. Tang, X. Chen, K. W. Leong, *Lab Chip* **2017**, *17*, 635–639.

[11] L. S. Roach, H. Song, R. F. Ismagilov, *Anal. Chem.* **2005**, 77, 785–796.

[12] N. Seeman, N. Kallenbach, *Biophys. J.* **1983**, *44*, 201–209.

[13] H. Yan, *Science* **2003**, *301*, 1882–1884.

[14] N. A. W. Bell, C. R. Engst, M. Ablay, G. Divitini, C. Ducati, T. Liedl, U. F. Keyser, *Nano Lett.* **2011**, *12*, 512–517.

[15] M. Langecker, V. Arnaut, T. G. Martin, J. List, S. Renner, M. Mayer, H. Dietz, F. C. Simmel, *Science* **2012**, *338*, 932–936.

[16] K. Göpfrich, C.-Y. Li, I. Mames, S. P. Bhamidimarri, M. Ricci, J. Yoo, A. Mames, A. Ohmann, M. Winterhalter, E. Stulz, A. Aksimentiev, U. F. Keyser, *Nano Lett.* **2016**, *16*, 4665–4669.

[17] E. S. Andersen, M. Dong, M. M. Nielsen, K. Jahn, R. Subramani, W. Mamdouh, M. M. Golas, B. Sander, H. Stark, C. L. P. Oliveira, J. S. Pedersen, V. Birkedal, F. Besenbacher, K. V. Gothelf, J. Kjems, *Nature* **2009**, *459*, 73–76.

[18] S. M. Douglas, I. Bachelet, G. M. Church, *Science* **2012**, *335*, 831–834.

[19] S. H. Park, P. Yin, Y. Liu, J. H. Reif, T. H. LaBean, H. Yan, *Nano Lett.* **2005**, *5*, 729–733.

[20] C. A. Mirkin, R. L. Letsinger, R. C. Mucic, J. J. Storhoff, *Nature* **1996**, *382*, 607–609.

[21] L. Parolini, J. Kotar, L. D. Michele, B. M. Mognetti, *ACS Nano* **2016**, *10*, 2392–2398.

[22] L. Feng, L.-L. Pontani, R. Dreyfus, P. Chaikin, J. Brujic, *Soft Matter* **2013**, *9*, 9816.

[23] Y. Zhang, A. McMullen, L.-L. Pontani, X. He, R. Sha, N. C. Seeman, J. Brujic, P. M. Chaikin, *Nat. Commun.* **2017**, *8* .

[24] D. Joshi, D. Bargteil, A. Caciagli, J. Burelbach, Z. Xing, A. S. Nunes, D. E. P. Pinto, N. A. M. Araujo, J. Brujic, E. Eiser, *Sci Adv.* **2016**, *2*, e1600881–e1600881.

[25] S.-Y. Teh, R. Lin, L.-H. Hung, A.P. Lee, *Lab Chip* **2008**, *8*, 198.

[26] K. Shohda, T. Toyota, T. Yomo, T. Sugawara, *ChemBioChem* **2003**, *4*, 778–781.

[27] A. Johnson-Buck, S. Jiang, H. Yan, N. G. Walter, *ACS Nano* **2014**, *8*, 5641–5649.

[28] J. Korlach, P. Schwille, W. W. Webb, G. W. Feigenson, *Proc. Natl. Acad. Sci. U. S. A.* **1999**, *96*, 8461–8466.

[29] C. Kurokawa, K. Fujiwara, M. Morita, I. Kawamata, Y. Kawagishi, A. Sakai, Y. Murayama, M Shin-ichiro, S. Nomura, S. Murata, M. Takinoue, M. Yanagisawa, *Proc. Natl. Acad. Sci. U. S. A.* **2017**, *114*, 7228–7233.

[30] F. Backouche, L. Haviv, D. Groswasser, A. Bernheim-Groswasser, *Phys. Biol*, **2006**, *3*, 264-273.

[31] A.-C. Reymann, R. Boujemaa-Paterski, J.-L. Martiel, C. Guerin, W. Cao, H. F. Chin, E. M. D. L. Cruz, M. Thery, L. Blanchoin, *Science*, **2012**, *336*, 1310-1314.

[32] S. K. Vogel, Z. Petrasek, F. Heinemann, P. Schwille, *eLife*, **2013**, *2*.

[33] E. Zamir, B. Geiger, Encyclopedia of Biological Chemistry (second edition), (Lennarz, W. J. and Lane, M. D., Eds.), Elsevier, Oxford. 2 318-323 **2013**.

[34] K. Göpfrich, I. Platzman, J. P. Spatz, *Trends in Biotechnol.* **2018**, *36* .

[35] M. He, J. S. Edgar, G. D. M. Jeffries, R. M. Lorenz, J. P. Shelby, D. T. Chiu, *Anal. Chem.* **2005**, *77*, 1539–1544.

[36] S. Köster, F. E. Angile, H. Duan, J. J. Agresti, A. Wintner, C. Schmitz, A. C. Rowat, C. A. Merten, D. Pisignano, A. D. Griffiths, D. A. Weitz, *Lab Chip* **2008**, *8*, 1110.

[37] E. Brouzes, M. Medkova, N. Savenelli, D. Marran, M. Twardowski, J. B. Hutchison, J. M. Rothberg, D. R. Link, N. Perrimon, M. L. Samuels, *Proc. Natl. Acad. Sci. U. S. A.* **2009**, *106*, 14195–14200.

[38] Y. Zeng, R. Novak, J. Shuga, M. T. Smith, R. A. Mathies, *Anal. Chem.* **2010**, *82*, 3183–3190.

[39] L. Mazutis, J. Gilbert, W. L. Ung, D. A. Weitz, A. D. Griffiths, J. A. Heyman, *Nat. Protoc.* **2013**, *8*, 870–891.

[40] T. P. Lagus, J. F. J. Edd, *Phys. D: Appl. Phys.* **2013**, *46*, 114005.

[41] V. Taly, B. T. Kelly, A. D. Griffiths, *ChemBioChem* **2007**, *8*, 263–272.

[42] M. Bikram, J. L. West, *Expert Opin. Drug Deliv.* **2008**, *5*, 1077–1091.

[43] R. Tewhey, J. B. Warner, M. Nakano, B. Libby, M. Medkova, P. H. David, S. K. Kotsopoulos, M. L. Samuels, J. B. Hutchison, J. W. Larson, E. J. Topol, M. P. Weiner, O. Harismendy, J. Olson, D. R. Link, K. A. Frazer, *Nat. Biotechnol.* **2009**, *27*, 1025–1031.

[44] R. K. Shah, J.-W. Kim, J. J. Agresti, D. A. Weitz, L.-Y. Chu, *Soft Matter* **2008**, *4*, 2303.

[45] P. C. Gach, K. Iwai, P. W. Kim, N. J. Hillson, A. K. Singh, *Lab Chip* **2017**, *17*, 3388–3400.

[46] https://eu.idtdna.com/calc/analyzer

[47] Y. Yan, J. I. L. Chen, D. S. Ginger, *Nano Lett.* **2012**, *12*, 2530–2536.

[48] J. Sharma, R. Chhabra, H. Yan, Y. Liu, *Chem. Commun.* **2007**, *5*, 477–479.

[49] D. Yao, H. Li, Y. Guo, X. Zhou, S. Xiao, H. Liang, *Chem. Commun.* **2016**, *52*, 7556–7559.

[50] S. Hernandez-Ainsa, M. Ricci, L. Hilton, A. Avino, R. Eritja, U. F. Keyser, *Nano Lett.* **2016**, *16*, 4462–4466.

[51] J. N. Zadeh, C. D. Steenberg, J. S. Bois, B. R. Wolfe, M. B. Pierce, A. R. Khan, R. M. Dirks, N. A. Pierce, *J. Comput. Chem.* **2010**, *32*, 170–173.

[52] J.-W. Janiesch, M. Weiss, G. Kannenberg, J. Hannabuss, T. Surrey, I. Platzman, J. P. Spatz, *Anal. Chem.* **2015**, *87*, 2063–2067.

[53] https://onlinelibrary.wiley.com/doi/abs/10.1002/bip.21615.

Chemical functionalization of microfluidic water-in-oil droplets is achieved via hydrophobic interactions of cholesterol-tagged DNA with the droplet-stabilizing surfactants. The DNA handle at the droplet periphery serves as a programmable binding site, which can carry an arbitrary group or compound. This method for reversible droplet functionalization is exemplified by attaching functional groups, beads, proteins and cells to the droplet periphery.

**Microfluidics**

K. Jahnke, M. Weiss, C. Frey, S. Antona, J.-W. Janiesch, I. Platzman, K. Göpfrich* and J. P. Spatz*

**Programmable functionalization of surfactant-stabilized microfuidic droplets via DNA-tags**